

Cite this: *J. Mater. Chem. C*, 2019,
7, 14493Received 10th October 2019,
Accepted 12th November 2019

DOI: 10.1039/c9tc05559b

rsc.li/materials-c

Solvothermal synthesis of cesium lead halide nanocrystals with controllable dimensions: a stoichiometry defined growth mechanism†

Min Chen,^{‡,ab} Huicheng Hu,^{‡,b} Nan Yao,^b Xiaolei Yuan,^{*a} Qixuan Zhong,^b
Muhan Cao,^{*b} Yong Xu^{id}^b and Qiao Zhang^{id}^{*b}

We presented here a solvothermal approach to synthesize CsPbX₃ nanostructures with precisely controlled dimensions. By simply varying the amount of Cs precursor, three-dimensional nanocubes, two-dimensional nanoplatelets/nanoribbons and one-dimensional nanorods with high uniformity in morphology and size were successfully synthesized. A stoichiometry defined growth mechanism has been proposed to explain the growth mechanism. This work not only adds another effective tool in the synthesis toolbox, but also helps to understand the formation mechanism of CsPbX₃ nanostructures.

Introduction

All inorganic perovskite CsPbX₃ (X = Cl, Br, and I) nanocrystals have been regarded as promising optoelectronic materials in recent years owing to their excellent photophysical properties, such as high photoluminescence quantum yield (PLQY), narrow emission linewidth, tunable emission wavelength covering the full visible range, high carrier mobility and long carrier diffusion length.^{1–7} They have attracted tremendous attention in diverse applications, including light emitting diodes (LEDs),^{8–12} solar cells,^{13,14} lasers^{15–17} and photodetectors.^{18–20} Since the geometric dimension of inorganic nanomaterials plays significant roles in determining their physicochemical properties, how to precisely control the dimensions of inorganic nanocrystals has been a hot topic in the field of nanoscience and nanotechnology. Over the past several years, researchers have demonstrated that CsPbX₃ nanocrystals with different geometric dimensions could show different photophysical and electronic properties which might

inspire some new applications.^{21–27} For example, three-dimensional (3D) CsPbX₃ nanocubes with high PLQY and narrow emission linewidth have shown promising potential as building blocks for high-performance optoelectronic nanodevices, such as LEDs, solar cells, lasers and X-ray detectors.^{11,17,23,27} Yang *et al.* reported that two-dimensional (2D) CsPbBr₃ nanoplatelets could be ideal candidates for blue LED devices due to the strong quantum confinement emission.²⁶ Tong *et al.* demonstrated that one-dimensional (1D) CsPbX₃ nanowires exhibited strongly polarized absorption and emission and thus can be integrated into nanoscale optoelectronic devices.²² To date, the dimensionally controlled synthesis of CsPbX₃ nanocrystals with various nanostructures has been achieved by adjusting the reaction parameters (such as time, temperature, precursor and surface ligands) in direct synthesis or post-modification approaches.^{26,28–35} However, it is quite challenging to make monodisperse CsPbX₃ nanocrystals with desired morphology in a simple and effective way. Since this field is still in its early stage, any new understanding or new findings will be very helpful and may further lead to a series of innovation in their practical application.

Solvothermal approach has proven to be an effective and powerful method to synthesize nanomaterials with controllable dimension and desired properties.^{36–40} Since our first report on solvothermal synthesis of CsPbX₃ nanocrystals in 2017,⁴¹ high-quality CsPbX₃ nanocrystals with various morphologies, such as nanocubes, nanowires, nanoplatelets and dodecapod nanoflowers, have been made through this approach.^{42–45} Different from the fast nucleation and growth kinetics of traditional hot-injection and re-precipitation methods, solvothermal method performs a relatively slow reaction that can provide a great opportunity to kinetically control the nucleation and growth process in the synthesis of nanocrystals so that the morphologies of product can be well defined. Moreover, solvothermal method has been featured for some unique properties, such as high crystallinity, high uniformity, precise control over the size and shape of products, and simple and scalable synthesis. In this study, we employed the solvothermal strategy to precisely control the dimensions of CsPbBr₃ nanostructures. By tuning the

^a School of Chemistry and Chemical Engineering, Nantong University, Nantong, 9 Seyuan Road, Nantong, 226019, Jiangsu, P. R. China.
E-mail: xlyuan@ntu.edu.cn

^b Institute of Functional Nano and Soft Materials (FUNSOM), Jiangsu Key Laboratory for Carbon-Based Functional Materials and Devices, Soochow University, 199 Ren'ai Road, Suzhou, 215123 Jiangsu, P. R. China.
E-mail: mhcao@suda.edu.cn, qiaozhang@suda.edu.cn

† Electronic supplementary information (ESI) available. See DOI: 10.1039/c9tc05559b

‡ These authors contributed equally for this work.

amount of cesium precursor, the dimension of CsPbBr₃ nanocrystals can be systematically manipulated from 3D nanocubes, 2D nanoplatelets and nanoribbons to 1D nanorods. Blue-shift of PL emission peak has been observed in those low dimensional CsPbBr₃ nanostructures because of the strong quantum confinement. Due to the anisotropic shape of low dimensional structures, the [0 0 *n*] (*n* = 1, 2, 3, 4, ...) planes which parallel to the lateral dimensions exhibited sharp peaks with strong intensity in their XRD patterns. The atomic ratio of cesium decreased gradually along with the shrinking of nanocrystals' dimension. A plausible stoichiometry defined growth mechanism has been proposed, in which the protonated octylamine can occupy Cs⁺ sites on nanocrystals surface more efficiently in the presence of lower concentration of Cs⁺, which can lower the surface energy, making it possible to evolve to low dimensional morphology. This proposed mechanism has been successfully extended to the preparation of CsPbX₃ nanocrystals with different halide compositions. This work not only provides a new approach in the controllable synthesis of CsPbX₃ nanocrystals with tunable dimension and morphology, but also sheds some light on the mechanism understanding of CsPbX₃ nanocrystals in the solvothermal synthesis approach.

Results and discussion

The synthesis of CsPbX₃ nanocrystals with controllable dimensions was performed through a solvothermal method. Briefly, certain volume of Cs precursor (0.15 M, 0.8 mL to 0.2 mL, see details in Table S1, ESI[†]) was added into PbBr₂ (0.025 M, 11 mL) solution containing oleic acid (OA), octylamine (OctAm) and 1-octadecene (ODE) at room temperature. The mixtures were then transferred into an autoclave and reacted at 120 °C for 60 minutes. The products were finally separated by centrifugation and washed with hexane. The synthesis details could be found in Experimental section in ESI[†]. TEM images show the morphological structures of CsPbBr₃ nanocrystals obtained by tuning the amount of Cs precursor. As depicted in Fig. 1 and Fig. S1 (ESI[†]), all products exhibited uniform morphology and size distribution, suggesting the high yield and high quality of these products. As shown in Fig. 1a and e, when 120 μmol Cs precursor was added, uniform 3D nanocubes with an average size of 12.3 nm were obtained. As the amount of Cs precursor decreased to 90 μmol and 60 μmol while the other parameters kept identical, monodisperse 2D nanoplatelets (Fig. 1b and f) and nanoribbons (Fig. 1c and g) with low contrast were obtained, respectively. The low contrast suggested the thin nature of products, which was confirmed by TEM images of nanocrystals assembled in a face-to-face manner (Fig. S1, ESI[†]). From their assembled morphology, it could be found that the thickness was around 3.0 nm. Since the unit cell of cubic CsPbBr₃ is about 0.58 nm, the thicknesses of 3.0 nm can be corresponded to 5 unit cells. Further decreasing the amount of Cs precursor to 30 μmol, 1D nanorods with longer length were obtained (Fig. 1d and h). Interestingly, CsPbBr₃ nanorods had a thickness of 3.0 nm, which was consistent with 2D nanoribbons and nanoplatelets

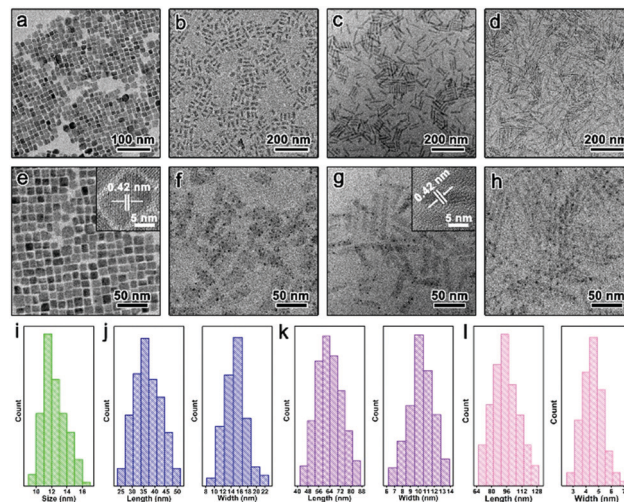


Fig. 1 (a–d) Low and (e–h) high magnification TEM images of CsPbBr₃: (a and e) nanocubes, (b and f) nanoplatelets, (c and g) nanoribbons and (d and h) nanorods obtained by tuning the amount of Cs precursor: 120 μmol, 90 μmol, 60 μmol and 30 μmol, while the other reaction parameters were kept identical. Insets in (e) and (g) are HRTEM images of CsPbBr₃ nanocubes and nanoribbons, respectively. (i–l) Histograms of side length and width distributions of CsPbBr₃ (i) nanocubes, (j) nanoplatelets, (k) nanoribbons and (l) nanorods.

(Fig. S1, ESI[†]). The corresponding size distribution histograms of different nanostructures were provided in Fig. 1i–l. The side lengths and side widths of products were 36.9 nm/15.0 nm (for nanoplatelets), 63.6 nm/10.2 nm (nanoribbons) and 94.7 nm/4.5 nm (nanorods), respectively (Table S1, ESI[†]). HRTEM images (insets in Fig. 1e and g) and their corresponding fast Fourier transform (FFT) patterns (Fig. S2 and S3, ESI[†]) confirmed a single-crystalline cubic feature of the nanocubes and nanoribbons. Furthermore, the lattice distances of nanocubes and nanoribbons were 0.42 nm, which can be assigned to the (110) planes of cubic phase.

UV-Vis absorption and PL emission spectra were used to investigate the optical properties of as-prepared CsPbBr₃ nanocrystals. As depicted in Fig. 2a, when 120 μmol of Cs precursor was employed, the as-obtained 3D CsPbBr₃ nanocubes showed a green color and a sharp emission peak at 516 nm, which was consistent with the previous reports.⁴⁶ In addition, CsPbBr₃ nanocubes showed an excitonic absorption peak at around 510 nm. As the amount of Cs precursor decreased, a remarkably large blue-shift in both absorption and emission peak was observed. This result could be attributed to the quantum confinement effect, in which the thickness of low dimensional structures (nanorods/nanoribbons/nanoplatelets) was smaller than their Bohr diameter (~7.0 nm).²¹ As shown in Fig. 2a, 2D CsPbBr₃ nanoplatelets and nanoribbons and 1D nanorods displayed very similar sharp PL emission peaks at around 460 nm, which can be corresponded to 5 perovskite unit cells as reported in previous works.^{26,47} Their excitonic absorption peaks were located at the same position *ca.* 446 nm. The sharp and narrow absorption peak indicated high uniformity of the product. The PL decay curves of all samples can be triexponential

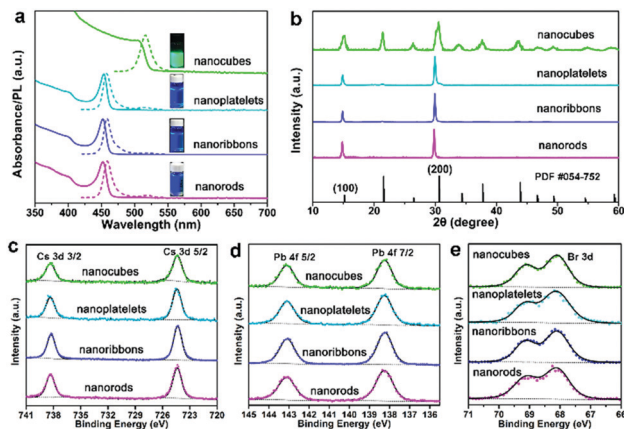


Fig. 2 (a) UV-Vis (solid) and PL emission (dash) spectra of CsPbBr₃ nanocrystals. The excitation wavelength is 365 nm. Bright digital images of colloidal CsPbBr₃ nanocrystals solution dispersed in hexane under UV light (365 nm) were shown in the insets in (a). (b) XRD patterns and (c–e) XPS spectra of CsPbBr₃ nanocrystals. The binding energies were calibrated with the C 1s peak of the free carbon (284.6 eV).

fitted well, as displayed in Fig. S4 (ESI[†]). The average lifetimes were determined to be 2.6 ns, 4.2 ns, 5.1 ns and 12.4 ns for nanorods, nanoribbons, nanoplatelets and nanocubes, respectively (Fig. S4 and Table S1, ESI[†]). The phase structures of all samples were confirmed by X-ray diffraction (XRD) analysis. As shown in Fig. 2b, the XRD signals of CsPbBr₃ nanocubes fitted well with the standard XRD patterns of cubic phase (JCPDS card# 054-752). The broad signal could be ascribed to the small particle size. Due to the anisotropic shape of the CsPbBr₃ nanoplatelets, the [0 0 *n*] (*n* = 1, 2, 3, 4, ...) planes which parallel to the lateral dimensions exhibited narrow peaks with high intensity. In contrast, the other peaks were much broader and less intense (see the enlarged XRD patterns in Fig. S5, ESI[†]). Interestingly, the peaks were slightly shifted toward low angles with respect to the standard diffraction pattern of cubic CsPbBr₃ phase, indicating a slight expansion of the overall lattice.^{32,47,48} The expanded lattice may come from the replacement of Cs⁺ ions by oleylammonium ions, which seems like an alkylammonium lead halide type like perovskite that could further slightly expand the lattice of nanocrystals.^{47,48} Similar phenomena were observed in CsPbBr₃ nanoribbons and nanorods. Only two XRD peaks at $2\theta = 14.8^\circ$ and 29.8° with high intensity were observed.

The surface chemistry of metal halide perovskites plays an important role on their morphology and size. X-ray photoelectron spectroscopy (XPS) analysis was performed to elucidate the surface properties of CsPbBr₃ nanocrystals with different

morphologies. The analysis of Cs 3d, Pb 4f and Br 3d peaks for each sample was shown in Fig. 2c–e, respectively. Based on the XPS analysis, the relative atomic ratios of Cs:Pb:Br for all samples were calculated and summarized in Table 1. The Cs:Pb ratio was found to be 0.99:1 in CsPbBr₃ nanocubes, which was close to the ideal 1:1 ratio in CsPbBr₃ structure. When the amount of Cs precursor decreased, the Cs:Pb ratio was gradually decreased and was lower than 1:1. For CsPbBr₃ nanoplatelets, nanoribbons and nanorods, the Cs:Pb:Br ratios were 0.90:1:2.60, 0.85:1:2.50 and 0.81:1:2.45, respectively. The amount of Cs precursor was found to significantly affect the surface component of as-obtained nanocrystals. Furthermore, the result suggested that our low dimensional nanocrystals had Cs deficiency on their surface which might be originated from the replacement of Cs⁺ by octylammonium ions. Previous literatures demonstrated that Cs cations on the surface of perovskites would be replaced by oleylammonium ions in the synthesis of 2D nanoplatelets and 1D nanowires, resulting in the Cs deficiency on their surface.^{24,47,49,50} The content of Cs, Pb and Br within the resulting products were further confirmed by energy dispersive X-ray (EDX) spectroscopy analysis. As shown in Table 1 and Fig. S6 (ESI[†]), the Cs:Pb:Br ratios were 1.00:1:2.83 (nanocubes), 0.91:1:2.62 (nanoplatelets), 0.85:1:2.60 (nanoribbons) and 0.82:1:2.50 (nanorods), respectively, which was in line with the XPS results. It should be noted that the low dimensional nanocrystals had a halide-deficient surface as well, which could be attributed to the increased surface-to-volume and decreased formation energy.^{25,49,51,52}

To further investigate the surface chemistry of our products, the aspect ratio (length/width) and surface-to-volume ratios for all samples were calculated. As shown in Fig. 3a, with the decreasing amount of Cs precursor, the aspect ratios of nanocrystals increased from 1.0 to 21.0. Additionally, as the Cs precursor decreased, the surface-to-volume ratio of nanocrystals increased. Thus, we can conclude that OctAm capping on the surface of perovskites can promote the anisotropic growth of nanocrystals during the synthesis of perovskites. Based on the above results, a possible formation mechanism was proposed (Fig. 3b). It has been widely accepted that the protonated OctAm by OA would compete with Cs⁺ cations in the formation of CsPbX₃ nanocrystals.^{24,47,53,54} When the concentration of Cs precursor was high, few Cs⁺ cations were replaced by octylammonium cations, resulting in the formation of isotropic shape of CsPbBr₃ nanocubes. When the amounts of Cs⁺ cations decreased, more protonated OctAm would locally mimic an octylammonium lead halide type cell. On the other hand, OctAm on the surface of nanocrystal would slow down the

Table 1 The relative atomic ratios of Cs:Pb:Br obtained from XPS and EDX, respectively

Elements	Nanocubes		Nanoplatelets		Nanoribbons		Nanorods	
	XPS	EDX	XPS	EDX	XPS	EDX	XPS	EDX
Cs(At%)	21.10	20.70	20.01	20.10	19.55	19.10	19.02	18.98
Pb(At%)	21.32	20.72	22.22	22.08	23.00	23.47	23.47	23.15
Br(At%)	57.58	58.58	57.77	57.82	57.45	58.43	57.51	57.87
Cs:Pb:Br	0.99:1:2.70	1.00:1:2.83	0.90:1:2.60	0.91:1:2.62	0.85:1:2.50	0.85:1:2.60	0.81:1:2.45	0.82:1:2.50

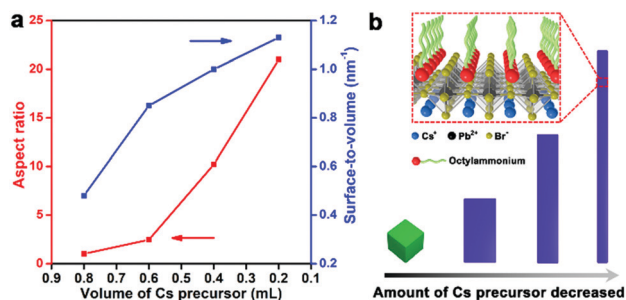


Fig. 3 (a) Aspect ratio (length/width) (red) and surface-to-volume (blue) relations as a function of the volume of Cs precursor added. (b) The possible proposed growth mechanism.

growth in vertical dimension and then limit the growth of vertical planes. As a result, thinner 2D nanoplatelets and nanoribbons could be obtained. When the concentration of Cs⁺ cations was very low, Cs⁺ cations were occupied by octylammonium cations more efficiently, which could lower the surface energy and further increase the specific surface area, resulting in the shrinking of dimension and formation of 1D nanorods. In order to further confirm the proposed mechanism, a series of experiments were performed (Table S2, ESI[†]). Firstly, when the amount of PbBr₂ was increased from 270 μmol to 406 μmol with fixed amount of Cs precursor (60 μmol), Cs⁺ cations can be replaced easier by octylammonium cations, which would limit the growth of nanocrystals in vertical dimension, leading to the morphology evolution from 2D nanoribbons to 1D nanorods (Fig. S7, ESI[†]). Furthermore, when the amount of PbBr₂ was decreased to 187 μmol, fewer Cs⁺ cations were replaced by octylammonium cations, resulting in the morphology evolution from 2D nanoribbons to CsPbBr₃ nanocubes (Fig. S8, ESI[†]).

Low dimensional CsPbX₃ nanostructures can be obtained by simply adding other lead halides or their mixtures (Cl, Cl/Br, or Br/I) in appropriate ratios (see more details in ESI[†]). On the surface of CsPbX₃ nanocrystals, octylammonium cations can occupy Cs⁺ cations and coordinate with halides on the surface. Since the binding energy of halides with octylammonium is different ($BE_{Cl^-} > BE_{Br^-} > BE_{I^-}$),⁵⁵ octylammonium cations can replace Cs⁺ cations more easily on the surface of CsPbCl₃ nanocrystals in comparison to CsPbBr₃ and CsPb(Br/I)₃ nanocrystals, leading to the generation of final morphologies from 1D nanorods, 2D nanoribbons to 2D nanoplatelets (Fig. 4a–f). The low dimensional CsPbX₃ nanocrystals dispersed in hexane showed bright emission from violet to green (Fig. 4g). The absorption and PL emission spectra showed slight red-shift with different halide compositions from chloride to bromide to iodide (Fig. 4h). It was worth pointing that, compared with CsPbCl₃ nanocubes emitting around 410 nm, 1D CsPbCl₃ nanorods exhibited a large blue-shift (~25 nm), which might be a good candidate for UV detector. The powder XRD patterns of low dimensional CsPbX₃ nanocrystals were shown in Fig. S9 (ESI[†]). The diffraction peaks of all samples can be indexed to cubic phase. In addition, two sharp and strong diffraction peaks correspond to (0 0 *n*) planes of cubic phase for all samples were observed, further confirming their anisotropic

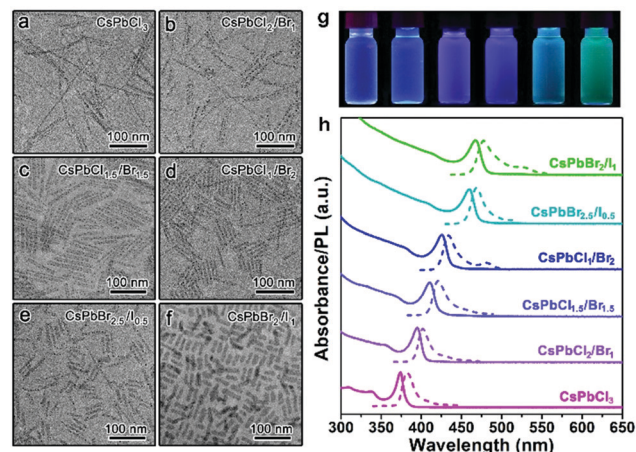


Fig. 4 (a–f) TEM images of low dimensional CsPbX₃ nanocrystals with different halide (X = Cl, Cl/Br and Br/I) compositions. (g) Digital photographs of colloidal dispersions of CsPbX₃ nanocrystals in hexane under UV light (365 nm) and (h) corresponding UV-vis (solid) and PL emission (dash) spectra of CsPbX₃ nanocrystals (λ_{exc} = 365 nm for all samples but 320 nm for CsPbCl₃).

nanostructure. Moreover, a slight blue-shift of the XRD peaks was observed with the halide changed from Cl⁻ to I⁻ (see enlarge XRD peaks in Fig. S9, ESI[†]), indicating the successful diffusion of halide ions in the lattice structures.

In addition, the emission of low dimensional CsPbX₃ nanostructures can be tuned by a fast anion exchange reaction at room temperature. Here we used CsPbX₃ nanoribbons as the example. As shown in Fig. 5a, 2D CsPbX₃ nanoribbons solution

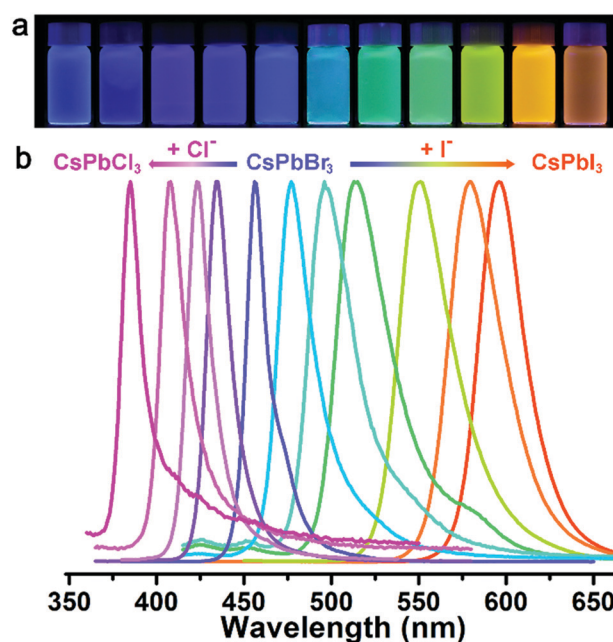


Fig. 5 (a) Photographs of CsPbX₃ nanoribbons dispersed in hexane prepared by mixing CsPbBr₃ nanoribbons solution with various concentrations of PbCl₂ or PbI₂ solution under UV light (λ = 365 nm) and (b) corresponding PL emission spectra of the halide-anion exchanged samples (λ_{exc} = 365 nm for all but 320 nm for CsPbCl₃, 400 nm for CsPbI₃).

with bright PL emission was obtained by mixing as-prepared CsPbBr₃ nanoribbons solution with PbX₂ (X = Cl and I) hexane solution. The PL emission spectra of CsPbX₃ nanoribbons could be tuned from 395 nm to 590 nm while maintaining narrow line widths of 10–35 nm from CsPbCl₃ to CsPbI₃ (Fig. 5b). The absorption spectra were varied from 370 nm to 580 nm with sharp peaks (Fig. S10, ESI[†]). It was obviously observed that a strong quantum confinement effect was still existed for all samples. The PL peak of CsPbCl₃ located at 395 nm, which blue-shifted about 15 nm compared to nanocubes (~410 nm). In addition, the PL emission peak of CsPbI₃ nanoribbons was significantly blue shifted (110 nm) compare to the CsPbI₃ nanocubes (~700 nm). Such large blue-shift in CsPbCl₃ and CsPbI₃ nanoribbons indicated the well-persevered morphology of nanoribbons, which was further confirmed by the TEM characterization (Fig. S11, ESI[†]).

Conclusions

In conclusion, we reported a solvothermal approach to synthesize CsPbX₃ nanocrystals with precisely controlled dimensions and high uniformity. By simply controlling the concentration of precursors, the morphologies of CsPbX₃ nanocrystals, including 3D nanocubes, 2D nanoplatelets/nanoribbons and 1D nanorods, could be well tuned. The 2D and 1D nanostructures showed a strong quantum confinement effect with a blue-shift in their PL emission and absorbance, which could create opportunities for applications in various fields. By using a combination of XPS and EDX characterizations, a plausible stoichiometry defined growth mechanism has been proposed. It is believed that the octylammonium ions would replace the Cs cations on the crystal surface, which limited the growth of vertical dimensions, leading to the formation of low-dimensional nanocrystals. Our approach not only added another effective tool in the toolbox for the synthesis of high-quality CsPbX₃ nanocrystals, but also provided a new perspective to control the dimension of CsPbX₃ nanocrystals, which might be extended to other materials, such as hybrid lead halide perovskite and lead-free perovskite nanocrystals.

Conflicts of interest

There are no conflicts to declare.

Acknowledgements

This work is supported by the National Natural Science Foundation of China (21673150, 21703146, 51802206, 51922073), Natural Science Foundation of Jiangsu Province (BK20180097, BK20180846). We acknowledge the financial support from the 111 Project, Collaborative Innovation Center of Suzhou Nano Science and Technology (NANO-CIC), the Priority Academic Program Development of Jiangsu Higher Education Institutions (PAPD), and Postgraduate Research & Practice Innovation Program of Jiangsu Province (KYCX19-1920).

References

- 1 Q. A. Akkerman, G. Raino, M. V. Kovalenko and L. Manna, *Nat. Mater.*, 2018, **17**, 394–405.
- 2 M. Cao, Y. Xu, P. Li, Q. Zhong, D. Yang and Q. Zhang, *J. Mater. Chem. C*, 2019, DOI: 10.1039/C9TC03978C.
- 3 M. V. Kovalenko, L. Protesescu and M. I. Bodnarchuk, *Science*, 2017, **358**, 745–750.
- 4 N. Pradhan, *J. Phys. Chem. Lett.*, 2019, **10**, 5847–5855.
- 5 J. Shamsi, A. S. Urban, M. Imran, L. De Trizio and L. Manna, *Chem. Rev.*, 2019, **119**, 3296–3348.
- 6 D. Yang, M. Cao, Q. Zhong, P. Li, X. Zhang and Q. Zhang, *J. Mater. Chem. C*, 2019, **7**, 757–789.
- 7 Q. Zhang and Y. Yin, *ACS Cent. Sci.*, 2018, **4**, 668–679.
- 8 K. Lin, J. Xing, L. N. Quan, F. P. G. de Arquer, X. Gong, J. Lu, L. Xie, W. Zhao, D. Zhang, C. Yan, W. Li, X. Liu, Y. Lu, J. Kirman, E. H. Sargent, Q. Xiong and Z. Wei, *Nature*, 2018, **562**, 245–248.
- 9 Z. Shi, S. Li, Y. Li, H. Ji, X. Li, D. Wu, T. Xu, Y. Chen, Y. Tian, Y. Zhang, C. Shan and G. Du, *ACS Nano*, 2018, **12**, 1462–1472.
- 10 Z. Shi, Y. Li, Y. Zhang, Y. Chen, X. Li, D. Wu, T. Xu, C. Shan and G. Du, *Nano Lett.*, 2017, **17**, 313–321.
- 11 J. Song, T. Fang, J. Li, L. Xu, F. Zhang, B. Han, Q. Shan and H. Zeng, *Adv. Mater.*, 2018, **30**, e1805409.
- 12 F. Zhang, Z. F. Shi, Z. Z. Ma, Y. Li, S. Li, D. Wu, T. T. Xu, X. J. Li, C. X. Shan and G. T. Du, *Nanoscale*, 2018, **10**, 20131–20139.
- 13 A. Swarnkar, A. R. Marshall, E. M. Sanehira, B. D. Chernomordik, D. T. Moore, J. A. Christians, T. Chakrabarti and J. M. Luther, *Science*, 2016, **354**, 92–95.
- 14 H. Bian, D. Bai, Z. Jin, K. Wang, L. Liang, H. Wang, J. Zhang, Q. Wang and S. Liu, *Joule*, 2018, **2**, 1500–1510.
- 15 Y. Wang, X. Li, J. Song, L. Xiao, H. Zeng and H. Sun, *Adv. Mater.*, 2015, **27**, 7101–7108.
- 16 Y. Wang, X. Li, V. Nalla, H. Zeng and H. Sun, *Adv. Funct. Mater.*, 2017, **27**, 1605088.
- 17 Z. Liu, J. Yang, J. Du, Z. Hu, T. Shi, Z. Zhang, Y. Liu, X. Tang, Y. Leng and R. Li, *ACS Nano*, 2018, **12**, 5923–5931.
- 18 C. Bao, J. Yang, S. Bai, W. Xu, Z. Yan, Q. Xu, J. Liu, W. Zhang and F. Gao, *Adv. Mater.*, 2018, **30**, e1803422.
- 19 P. Ramasamy, D. H. Lim, B. Kim, S. H. Lee, M. S. Lee and J. S. Lee, *Chem. Commun.*, 2016, **52**, 2067–2070.
- 20 Z. Yang, M. Wang, H. Qiu, X. Yao, X. Lao, S. Xu, Z. Lin, L. Sun and J. Shao, *Adv. Funct. Mater.*, 2018, **28**, 1705908.
- 21 L. Protesescu, S. Yakunin, M. I. Bodnarchuk, F. Krieg, R. Caputo, C. H. Hendon, R. X. Yang, A. Walsh and M. V. Kovalenko, *Nano Lett.*, 2015, **15**, 3692–3696.
- 22 Y. Tong, B. J. Bohn, E. Bladt, K. Wang, P. Muller-Buschbaum, S. Bals, A. S. Urban, L. Polavarapu and J. Feldmann, *Angew. Chem., Int. Ed.*, 2017, **56**, 13887–13892.
- 23 Q. Chen, J. Wu, X. Ou, B. Huang, J. Almutlaq, A. A. Zhumekenov, X. Guan, S. Han, L. Liang, Z. Yi, J. Li, X. Xie, Y. Wang, Y. Li, D. Fan, D. B. L. Teh, A. H. All, O. F. Mohammed, O. M. Bakr, T. Wu, M. Bettinelli, H. Yang, W. Huang and X. Liu, *Nature*, 2018, **561**, 88–93.

- 24 X. Sheng, G. Chen, C. Wang, W. Wang, J. Hui, Q. Zhang, K. Yu, W. Wei, M. Yi, M. Zhang, Y. Deng, P. Wang, X. Xu, Z. Dai, J. Bao and X. Wang, *Adv. Funct. Mater.*, 2018, **28**, 1800283.
- 25 Y. Wu, C. Wei, X. Li, Y. Li, S. Qiu, W. Shen, B. Cai, Z. Sun, D. Yang, Z. Deng and H. Zeng, *ACS Energy Lett.*, 2018, **3**, 2030–2037.
- 26 D. Yang, Y. Zou, P. Li, Q. Liu, L. Wu, H. Hu, Y. Xu, B. Sun, Q. Zhang and S.-T. Lee, *Nano Energy*, 2018, **47**, 235–242.
- 27 J. Yuan, X. Ling, D. Yang, F. Li, S. Zhou, J. Shi, Y. Qian, J. Hu, Y. Sun, Y. Yang, X. Gao, S. Duhm, Q. Zhang and W. Ma, *Joule*, 2018, **2**, 2450–2463.
- 28 D. Zhang, S. W. Eaton, Y. Yu, L. Dou and P. Yang, *J. Am. Chem. Soc.*, 2015, **137**, 9230–9233.
- 29 S. Sun, D. Yuan, Y. Xu, A. Wang and Z. Deng, *ACS Nano*, 2016, **10**, 3648–3657.
- 30 G. Almeida, L. Goldoni, Q. Akkerman, Z. Dang, A. H. Khan, S. Marras, I. Moreels and L. Manna, *ACS Nano*, 2018, **12**, 1704–1711.
- 31 Y. Dong, T. Qiao, D. Kim, D. Parobek, D. Rossi and D. H. Son, *Nano Lett.*, 2018, **18**, 3716–3722.
- 32 L. Peng, A. Dutta, R. Xie, W. Yang and N. Pradhan, *ACS Energy Lett.*, 2018, **3**, 2014–2020.
- 33 J. K. Sun, S. Huang, X. Z. Liu, Q. Xu, Q. H. Zhang, W. J. Jiang, D. J. Xue, J. C. Xu, J. Y. Ma, J. Ding, Q. Q. Ge, L. Gu, X. H. Fang, H. Z. Zhong, J. S. Hu and L. J. Wan, *J. Am. Chem. Soc.*, 2018, **140**, 11705–11715.
- 34 S. K. Mehetor, H. Ghosh and N. Pradhan, *ACS Energy Lett.*, 2019, **4**, 1437–1442.
- 35 D. Yang, P. Li, Y. Zou, M. Cao, H. Hu, Q. Zhong, J. Hu, B. Sun, S. Duhm, Y. Xu and Q. Zhang, *Chem. Mater.*, 2019, **31**, 1575–1583.
- 36 G. Demazeau, *J. Mater. Sci.*, 2007, **43**, 2104–2114.
- 37 D. R. Modeshia and R. I. Walton, *Chem. Soc. Rev.*, 2010, **39**, 4303–4325.
- 38 L. Zhang, W. Niu and G. Xu, *Nano Today*, 2012, **7**, 586–605.
- 39 J. Lai, W. Niu, R. Luque and G. Xu, *Nano Today*, 2015, **10**, 240–267.
- 40 S. P. Sasikala, P. Poulin and C. Aymonier, *Adv. Mater.*, 2017, **29**, 1605473.
- 41 M. Chen, Y. Zou, L. Wu, Q. Pan, D. Yang, H. Hu, Y. Tan, Q. Zhong, Y. Xu, H. Liu, B. Sun and Q. Zhang, *Adv. Funct. Mater.*, 2017, **27**, 1701121.
- 42 M. Chen, H. Hu, Y. Tan, N. Yao, Q. Zhong, B. Sun, M. Cao, Q. Zhang and Y. Yin, *Nano Energy*, 2018, **53**, 559–566.
- 43 Z.-J. Li, E. Hofman, A. H. Davis, A. Khammang, J. T. Wright, B. Dzikovski, R. W. Meulenberg and W. Zheng, *Chem. Mater.*, 2018, **30**, 6400–6409.
- 44 W. Zhai, J. Lin, C. Li, S. Hu, Y. Huang, C. Yu, Z. Wen, Z. Liu, Y. Fang and C. Tang, *Nanoscale*, 2018, **10**, 21451–21458.
- 45 W. Zhai, J. Lin, Q. Li, K. Zheng, Y. Huang, Y. Yao, X. He, L. Li, C. Yu, C. Liu, Y. Fang, Z. Liu and C. Tang, *Chem. Mater.*, 2018, **30**, 3714–3721.
- 46 L. Wu, H. Hu, Y. Xu, S. Jiang, M. Chen, Q. Zhong, D. Yang, Q. Liu, Y. Zhao, B. Sun, Q. Zhang and Y. Yin, *Nano Lett.*, 2017, **17**, 5799–5804.
- 47 Q. A. Akkerman, S. G. Motti, A. R. Srimath Kandada, E. Mosconi, V. D'Innocenzo, G. Bertoni, S. Marras, B. A. Kamino, L. Miranda, F. De Angelis, A. Petrozza, M. Prato and L. Manna, *J. Am. Chem. Soc.*, 2016, **138**, 1010–1016.
- 48 J. Shamsi, P. Rastogi, V. Caligiuri, A. L. Abdelhady, D. Spirito, L. Manna and R. Krahne, *ACS Nano*, 2017, **11**, 10206–10213.
- 49 D. Zhang, Y. Yu, Y. Bekenstein, A. B. Wong, A. P. Alivisatos and P. Yang, *J. Am. Chem. Soc.*, 2016, **138**, 13155–13158.
- 50 B. J. Bohn, Y. Tong, M. Gramlich, M. L. Lai, M. Doblinger, K. Wang, R. L. Z. Hoyer, P. Muller-Buschbaum, S. D. Stranks, A. S. Urban, L. Polavarapu and J. Feldmann, *Nano Lett.*, 2018, **18**, 5231–5238.
- 51 Y. Cai, L. Wang, T. Zhou, P. Zheng, Y. Li and R. J. Xie, *Nanoscale*, 2018, **10**, 21441–21450.
- 52 W. van der Stam, J. J. Geuchies, T. Altantzis, K. H. van den Bos, J. D. Meeldijk, S. Van Aert, S. Bals, D. Vanmaekelbergh and C. de Mello Donega, *J. Am. Chem. Soc.*, 2017, **139**, 4087–4097.
- 53 D. Amgar, A. Stern, D. Rotem, D. Porath and L. Etgar, *Nano Lett.*, 2017, **17**, 1007–1013.
- 54 T. Udayabhaskararao, M. Kazes, L. Houben, H. Lin and D. Oron, *Chem. Mater.*, 2017, **29**, 1302–1308.
- 55 B. Cherng and F.-M. Tao, *J. Chem. Phys.*, 2001, **114**, 1720–1726.